Geophysical Research Letters

RESEARCH LETTER
10.1029/2023GL107429

Quantifying Seasonal and Diurnal Cycles of Solar-Induced Fluorescence With a Novel Hyperspectral Imager

Sophie Ruehr[1,2], Cynthia Gerlein-Safdi[2,3], Nicola Falco[2], Paul O. Seibert[2,3], Chunwei Chou[2], Loren Albert[4], and Trevor F. Keenan[1,2]

[1]Department of Environmental Science, Policy & Management, UC Berkeley, Berkeley, CA, USA, [2]Climate & Ecosystem Sciences Division, Lawrence Berkeley National Laboratory, Berkeley, CA, USA, [3]Department of Civil and Environmental Engineering, UC Berkeley, Berkeley, CA, USA, [4]Department of Forest Ecosystems & Society, Oregon State University, Corvallis, OR, USA

Key Points:

- Novel imagery technology enables solar-induced fluorescence (SIF) acquisition across space and time
- SIF diurnal and seasonal variations correspond to carbon fluxes and environmental conditions
- Imaging capacity predicts leaf-level physiology across leaf, plant, and landscape scales

Supporting Information:

Supporting Information may be found in the online version of this article.

Correspondence to:

S. Ruehr,
sophie_ruehr@berkeley.edu

Citation:

Ruehr, S., Gerlein-Safdi, C., Falco, N., Seibert, P. O., Chou, C., Albert, L., & Keenan, T. F. (2024). Quantifying seasonal and diurnal cycles of solar-induced fluorescence with a novel hyperspectral imager. *Geophysical Research Letters*, *51*, e2023GL107429. https://doi.org/10.1029/2023GL107429

Received 4 DEC 2023
Accepted 14 JUL 2024

Author Contributions:

Conceptualization: Cynthia Gerlein-Safdi, Nicola Falco
Data curation: Nicola Falco
Formal analysis: Sophie Ruehr
Funding acquisition: Trevor F. Keenan
Investigation: Paul O. Seibert, Chunwei Chou
Methodology: Sophie Ruehr, Cynthia Gerlein-Safdi, Nicola Falco
Resources: Chunwei Chou
Software: Sophie Ruehr, Cynthia Gerlein-Safdi
Supervision: Trevor F. Keenan
Visualization: Sophie Ruehr
Writing – original draft: Sophie Ruehr
Writing – review & editing: Sophie Ruehr, Cynthia Gerlein-Safdi, Nicola Falco, Paul O. Seibert,

Abstract Solar-induced fluorescence (SIF) is a proxy of ecosystem photosynthesis that often scales linearly with gross primary productivity (GPP) at the canopy scale. However, the mechanistic relationship between GPP and SIF is still uncertain, especially at smaller temporal and spatial scales. We deployed a ultra-hyperspectral imager over two grassland sites in California throughout a soil moisture dry down. The imager has high spatial resolution that limits mixed pixels, enabling differentiation between plants and leaves within one scene. We find that imager SIF correlates well with diurnal changes in leaf-level physiology and gross primary productivity under well-watered conditions. These relationships deteriorate throughout the dry down event. Our results demonstrate an advancement in SIF imaging with new possibilities in remotely sensing plant canopies from the leaf to the ecosystem. These data can be used to resolve outstanding questions regarding SIF's meaning and usefulness in terrestrial ecosystem monitoring.

Plain Language Summary Estimating the rate of carbon uptake by vegetation across space and time remains a challenge. Solar-induced fluorescence (SIF), the emission of light by vegetation during photosynthesis, has recently emerged as a potential estimate of carbon uptake in many ecosystems and is observable from both satellites and ground-based sensors. Here we present results from a field campaign with a novel SIF instrument that creates images (akin to a photo) across a landscape, allowing for SIF measurements from individual leaves, plants, or areas of interest. We find that SIF retrievals from the imager correspond to seasonal variations in carbon dioxide fixation rates and leaf-level physiology relating to photosynthesis. We use this novel technology to improve understanding of SIF and carbon uptake across spatial and temporal scales.

1. Introduction

Estimating rates of carbon fixation remains a challenge in quantifying and predicting the global carbon cycle. Recently, solar-induced fluorescence (SIF) has emerged as a powerful tool in monitoring photosynthesis and plant response to water stress (Mohammed et al., 2019; Sun, Gu, et al., 2023). A small portion (0%–2%) of energy absorbed by chlorophyll is reemitted as fluorescence at longer wavelengths. The magnitude of this signal is related to rates of carbon assimilation in plants (Porcar-Castell et al., 2014). SIF has been shown to scale linearly with gross primary productivity (GPP) at the canopy scale across multiple biomes (Li et al., 2018; Sun et al., 2017). Since the rate of electron transfer within chloroplasts is dependent on water availability, SIF also provides information on plant physiological response to water stress (Liu et al., 2018; Paynter et al., 2020; Wang et al., 2016). Unlike vegetation indices, such as the normalized difference vegetation index (NDVI), which requires change in either structural properties or chlorophyll concentration before change is detected, SIF has been shown to reflect the downregulation of photosynthesis in real-time, making it a useful tool with which to study the carbon cycle and ecosystem response to environmental stressors (Liu et al., 2018; J. Zhang et al., 2022).

Incoming photons captured by chlorophyll pigments are partitioned into various pathways within the leaf. These include photochemistry, non-photochemical quenching, and fluorescence emission (Mohammed et al., 2019; Porcar-Castell et al., 2014). The proportion of photons directed towards each pathway varies with environmental conditions and plant physiology. For example, leaf-scale observations from evergreen forests suggest that the relationship between photosystem II efficiency (Φ_{PSII}) and fluorescence yield is irradiance-dependent and nonlinear (Maguire et al., 2020; van der Tol et al., 2016). The partitioning of photons between pathways also introduces non-linearities into the carbon reactions of photosynthesis, partially decoupling GPP and SIF over

Chunwei Chou, Loren Albert, Trevor F. Keenan

short temporal and spatial scales (Magney et al., 2020; Marrs et al., 2020; Martini et al., 2022; Simmer et al., 2015; Verma et al., 2017).

Further study is needed to resolve inconsistencies in the SIF-GPP relationship across multiple spatial and temporal scales, including scaling from the leaf to canopy (He et al., 2020; Magney et al., 2020; Mohammed et al., 2019; Pierrat et al., 2024; Simmer et al., 2015). Specifically, a larger body of experimental and observational data would resolve open questions regarding the interpretation of SIF. These questions relate to leaf-level photochemistry, the proportion of fluoresced photons that ultimately reach detectors through canopies, and spatial and temporal scaling from the site-level to satellite observation platforms (Sun, Gu, et al., 2023; Sun, Wen, et al., 2023).

The majority of hyperspectral sensors deployed for time series integrate reflectance spectra over a footprint, resulting in SIF estimates that do not resolve fine spatial variation. Recently, however, a new generation of imaging sensors has been developed. These instruments have been deployed from aircraft to quantify SIF over agricultural lands (Frankenberg et al., 2018; Paynter et al., 2020; Rascher et al., 2015), experimental plots (Rossini et al., 2015), and in comparison with satellite imagery (Maguire et al., 2021). The majority of these imaging campaigns have not considered the relationship of leaf-level physiology to SIF imaging retrievals (Frankenberg et al., 2018; Paynter et al., 2020; Rossini et al., 2015) or the effects of seasonal and diurnal cycles on SIF acquisitions (Rascher et al., 2015). Increased attention to diurnal, seasonal, and environmental covariates is essential to improving understanding of SIF and its uncertainties over space and time (Porcar-Castell et al., 2021; Sun, Wen, et al., 2023).

Here we present results from multiple deployments of a high-resolution hyperspectral chlorophyll fluorescence imager (Headwall Photonics, Fitchburg, MA, USA), one of the first commercially available SIF imagers, in spring 2022 at two grassland sites in California over the course of diurnal and seasonal cycles. The field sites are outfitted with meteorological monitoring equipment and, at one site, an eddy covariance flux tower. Diurnal leaf-level physiology measurements were collected throughout the field campaign. We first discuss SIF retrieval algorithms and a sensitivity analysis of retrieval parameters. We then consider relationships between SIF acquisitions, leaf-level physiology, and environmental conditions. Our goal is to demonstrate the potential of such ground-based field measurements to resolve current knowledge gaps and new approaches in the study of SIF (Sun, Gu, et al., 2023).

2. Field Methods

2.1. Grassland Sites

The imager was deployed at two grassland sites in California in spring 2022. At both sites, the understory low-lying grasses green up during the winter wet season (November-April) and then senesce as soil moisture declines during the dry season (May-October). The first site, the Sensors at Mesoscale with Autonomous Remote Telemetry (SMART) Soils Testbed, is the focus of this study. Adjacent to Lawrence Berkeley National Lab in Berkeley, CA, the testbed is a unique experimental setup that enables high-precision monitoring in a controlled environment. The imager was deployed on five different acquisition dates in April and May 2022 (2022-04-18, 2022-05-03, 2022-05-09, 2022-05-17, and 2022-05-24) with the same geometry (centered on the testbed, with the same field of view, viewing angle and at the same height, Figure 1) during clear-sky conditions. The majority of the following analyses focus on data collected at the SMART testbed. The second site, Tonzi Ranch, is used for a brief complementary analysis of SIF imager acquisitions and ecosystem carbon fluxes. Tonzi Ranch is a Mediterranean oak savanna with an existing AmeriFlux eddy covariance tower (Ma et al., 2016). The imager was deployed on one sunny day (2022-05-04) with the objective of comparing diurnal cycles of carbon fluxes, along with other environmental variables, to SIF imager acquisitions. Additional information on the Tonzi Ranch site and instrumentation can be found im the in Supporting Information S1.

The SMART testbed (Figure 1) housed a rectangular volume (with dimensions of 4.7 (length) x 1.2 (width) x 1.0 (height) m) of loamy soil obtained from Hopland, CA. Testbed vegetation in spring 2022 grew from seeds pre-existing in the soil and comprised various species including thistle (*Carduus pycnocephalus*, C_3), dock (*Rumex crispus*, C_3), and grass (*Melica californica*, C_3). A Phenocam (NetCam SC, Stardot, USA) was used to track the greening and senescence of the vegetation. Wind speed, air temperature, vapor pressure deficit, and precipitation were measured at half-hourly intervals 3 m above the soil surface by a weather station (ATMOS 41, Meter,

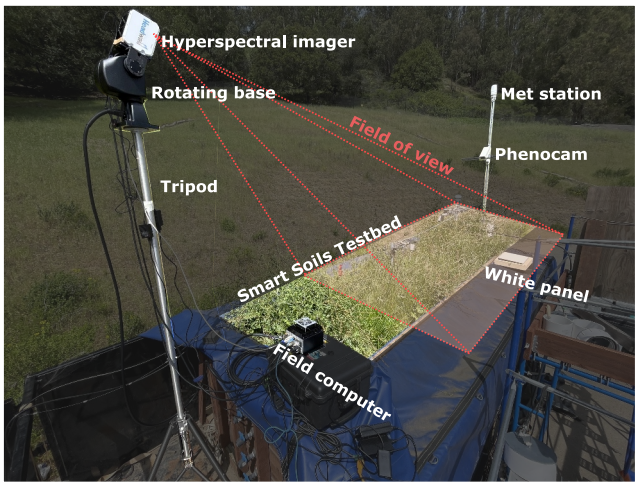

Figure 1. Smart Soils Testbed deployment setup. The hyperspectral imager was mounted with a −20° viewing angle on a rotating base, which operated the push broom sensor, above a tripod. The instrumentation was controlled by a field computer. The field of view included grasses within the testbed and a white reference panel. A meteorological station recorded half-hourly environmental conditions and a Phenocam took daily RGB photos of the grasses in the testbed. A similar setup was used at Tonzi Ranch.

Germany). Incoming photosynthetic photon flux density (PPFD) was measured at 1.5 m above the soil surface by a quantum sensor (SQ-521, Apogee, USA), and soil moisture was measured by 10 soil sensors (TEROS 12, Meter, Germany) at five depths (−0.05, −0.1, −0.3, −0.5, −0.7 m) at two lateral locations. Time series of the variables aggregated to daily intervals are shown in Figure S1 in Supporting Information S1. Besides a small input of precipitation in mid-April, no water was added to the testbed, resulting in a progressive soil moisture dry down (Figure 3).

Hyperspectral images were collected every half-hour from approximately 11:00 to 14:30 once a week from 18 April 2022 to 25 May 2022, when the plants had fully senesced. Meanwhile, leaf-level physiological measurements were collected two or three times throughout the day with a handheld fluorometer (Li-600, LICOR Biosciences, USA) on several individual plants, which were tracked throughout the growing season. The fluorometer measured minimum fluorescence (700–780 nm) under natural sunlight (Fs) and maximum fluorescence under a saturating flash (Fm'). Φ_{PSII} is calculated as:

$$\Phi_{PSII} = \frac{Fm' - Fs}{Fm'} \quad (1)$$

2.2. Instrument Details and Field Protocol

The Headwall hyperspectral imager is a push-broom scanner characterized by 1,600 spatial channels, a spectral range of 670–780 nm, a full width at half maximum of 0.1–0.2 nm, and a spectral sampling interval of 0.051 nm/pixel (Figure S2 in Supporting Information S1). The instrument, which has very fine spectral resolution (≤0.2 nm full width at half maximum), displays improved relationships with leaf-level SIF measurements when compared with broader-band instruments (Belwalkar et al., 2021) and, under well-lit conditions and with adequate exposure time, can detect differences in SIF due to phenology in broadleaf trees (Porcar-Castell et al., 2021).

The imager was mounted on a rotating base (Teledyne FLIR pan-tilt unit, D100 E, FLIR Cameras, Middletown, NY), which rotates horizontally to scan the scene. The spatial resolution of the resulting image is determined by rotation speed and frame rate (width of the image), as well as distance to target (footprint). The imager and rotating base were mounted on a 2-m tripod with a viewing angle of −20°. Although a nadir view would have been preferable to minimize the effects of viewing angle, the rotating base was only capable of a maximum of −20° downward rotation. Images were collected under only clear-sky conditions. Changes in atmospheric composition indiscernible to the naked eye, including thin high altitude cloud cover or haze, may have been present during acquisitions. The imager is not weatherproof for long-term installations, requiring it to be set up and taken down each day of acquisitions.

Signal-to-noise ratios were calculated for a similar instrument of the same model from Headwall Photonics by (Paynter et al., 2020), which found a strong ($R^2 = 0.997$) nonlinear relationship between radiance and noise of

$$\sigma = 365.99 \ \text{radiance}^{0.5295} \quad (2)$$

where σ is the absolute noise. This signal-to-noise ratio, combined with the instrument's high spectral resolution, allows for improved quantification of absolute SIF and O_2-A band depth, as well as stronger relationships with leaf-level SIF, when compared with broader-band instruments (Belwalkar et al., 2021).

Shot noise, a function of light intensity, is present, and atmospheric noise is also present in any measurement taken at a distance. Spectral stray light was shown to have minimal effects on SIF retrieval using data from a sensor of the same make/model, provided that the target and reference spectra are both collected with the same sensor (Albert et al., 2023). Spatial stray light has not yet been characterized for the specific instrument deployed for this project; however, as neighboring pixels were averaged, the effect of spatial stray light should be reduced.

10.1029/2023GL107429

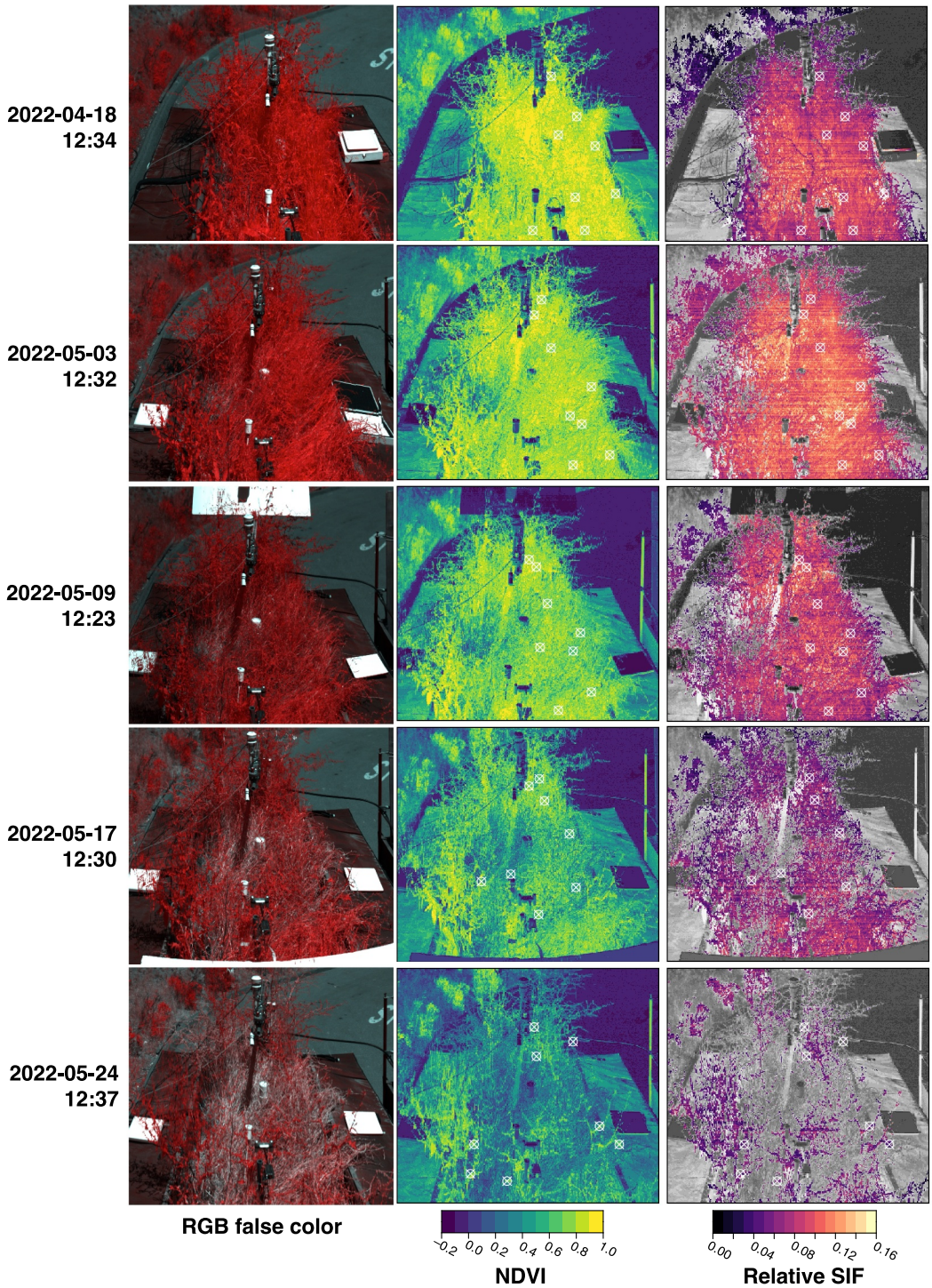

Figure 2. Testbed senescence observed by the imager at midday from 2022 to 04–18 to 2022-05-24. **Left column:** False-color RGB images (R = 780, G = 670, G = 670 nm). **Center column:** NDVI images. **Right column:** Relative SIF (unitless, %) masked out where NDVI (greyscale) and NIR are low (<0.5 and <8 mW cm^{-2} μm^{-1} sr^{-1}, respectively). White crosses mark matched locations of leaf-level LICOR Li-600 measurements. Image footprints on the testbed are approximately 2.25 m wide x 3.5 m deep, with pixel size = ~0.5 cm. The imager setup, viewing angle, height, and field of view remain the same for each day of acquisitions.

10.1029/2023GL107429

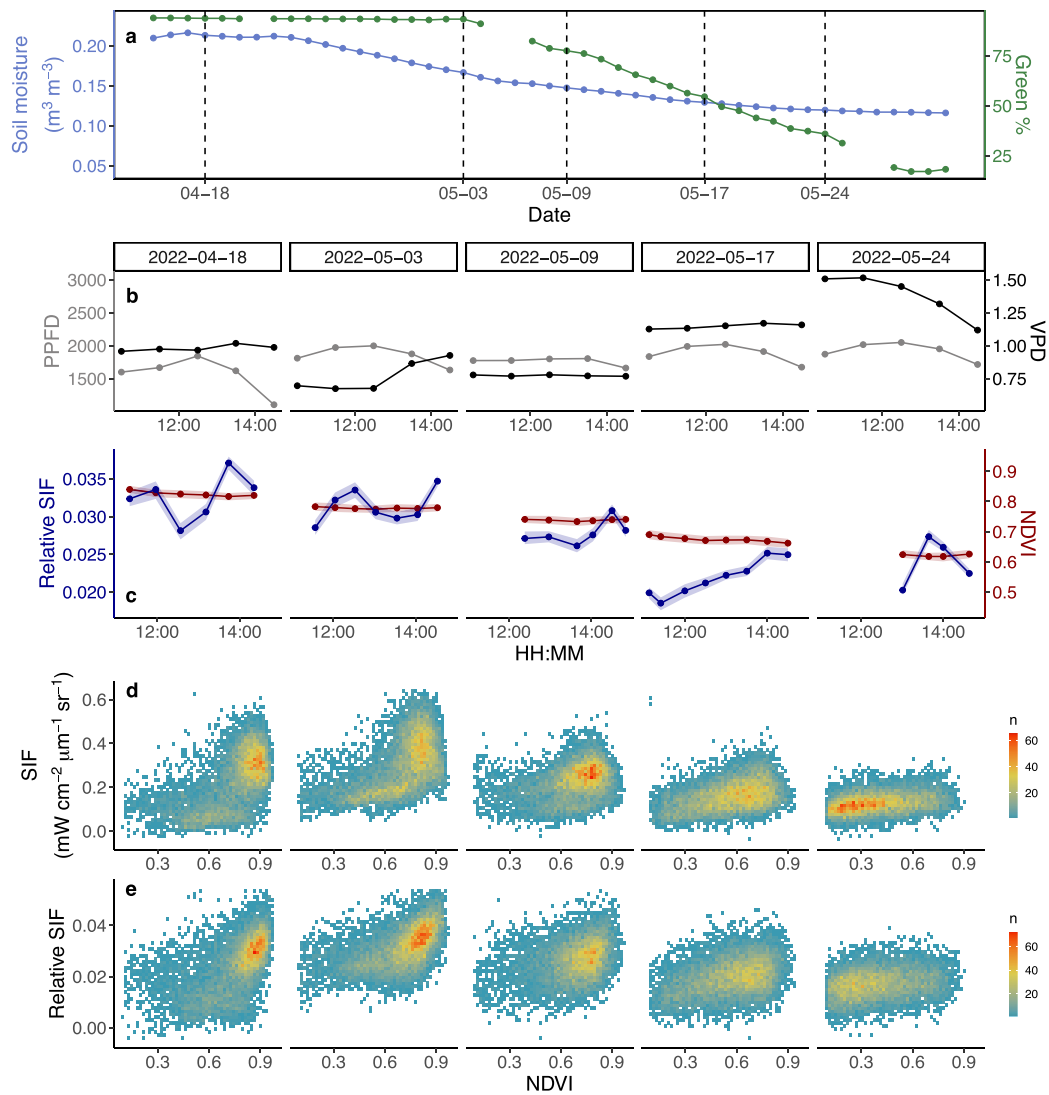

Figure 3. Seasonal (a) and diurnal (b)-(e) variations in meteorological conditions, NDVI, SIF, and relative SIF at the testbed. (a) Daily soil moisture (m^3 m^{-3}, blue) and green percentage as observed by the Phenocam (%, green) from 2022 to 04–15 to 2022-06-01, with dashed vertical lines marking dates of SIF imager deployment. (b) Lines and points show photosynthetic photon flux density (PPFD (μmol m^{-2} s^{-1}), gray) and vapor pressure deficit (VPD (kPa), black) over the course of the day and season. (c) Lines and points show median relative SIF (%) (blue) and NDVI (red) with 45–55th quantiles (shading), representing relative spread within images. (d),(e) Density (n) plots of NDVI versus SIF (d) and relative SIF (e) over the course of the season with color scale indicating density count.

Non-linear radiometric calibration was implemented by Headwall during factory calibration in June 2021 using a Labsphere integrating sphere illuminated by a QTH source, which is traceable to NIST. Dark calibration and exposure (camera integration time) adjustments were performed prior to each image acquisition. Exposure was adjusted such that the radiance of the white panel (12" Spectralon, Edmund Optics, Barrington, NJ, USA) was approximately 15% below saturation to avoid clipping distortion (Fu et al., 2021). After setting degrees of horizontal rotation to capture the desired area of interest, the rotation rate and frame speed were adjusted to ensure square pixels. For each image, the reference white panel, which is required for the SIF retrieval we employed (Section 2.3), was placed adjacent to the area of interest and within the field of view (Figure 1).

Additional corrections and calibrations, including geometric correction and instrument calibrations and corrections not implemented by the Headwall software, were not undertaken for this study. How to best correct for the

10.1029/2023GL107429

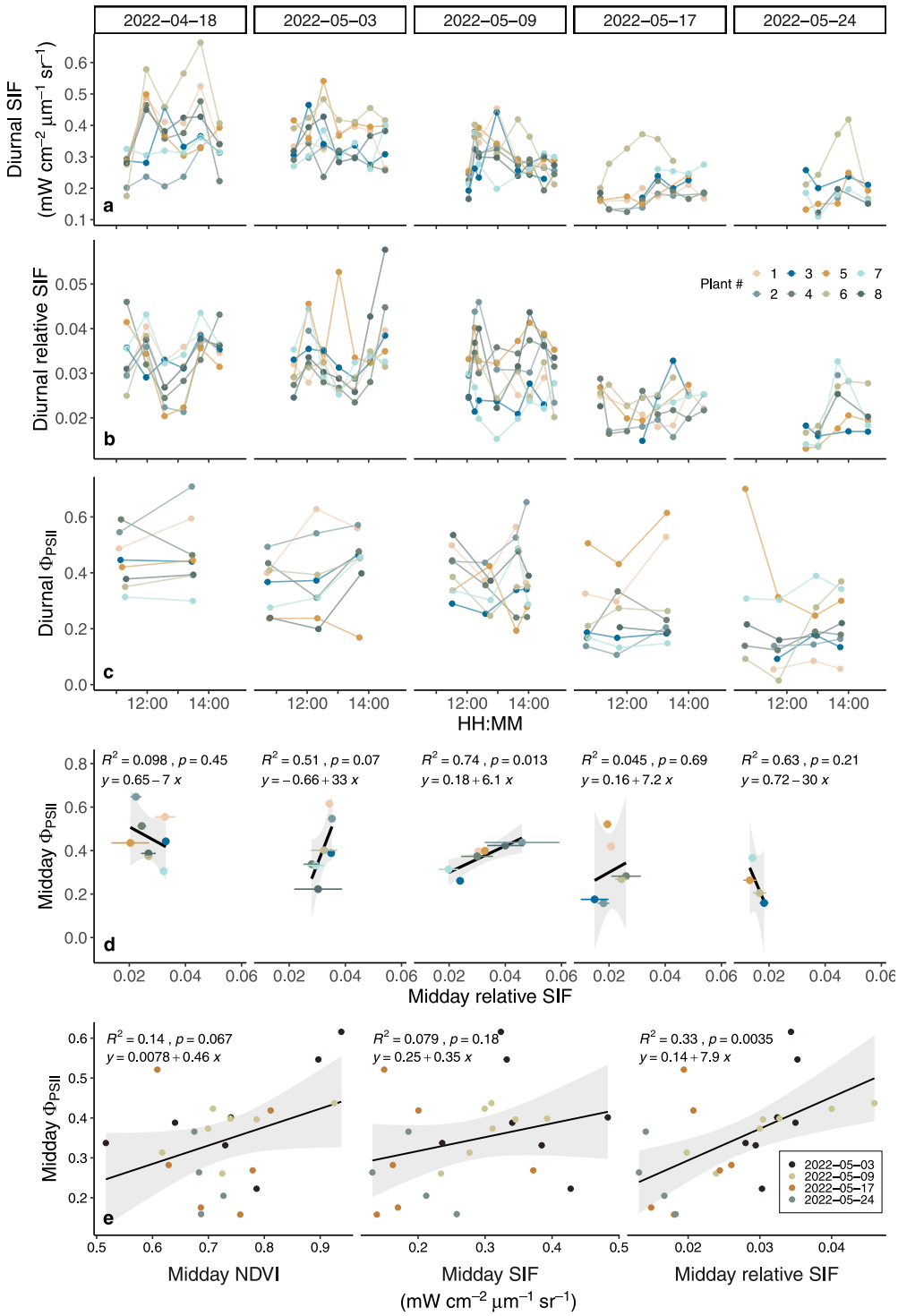

Figure 4. Comparison of leaf-level physiology to imager SIF retrievals on five dates over the course of the dry down (2022-04-18 to 2022-5-24). Diurnal cycles of (a) SIF (mW cm^{-2} μm^{-1} sr^{-1}) and (b) relative SIF (%) extracted from pixels corresponding to leaf-level measurements of (c) photosystem II efficiency (Φ_{PSII}) with a LiCOR Li-600 on eight individual plants (colors). (d) Relative SIF versus leaf-level Φ_{PSII} at midday on 5 days, with linear regression (lines) and error (shading), with respective equations, R^2, and p-values. Horizontal lines show relative SIF range within each bilinearly extracted point. (e) Midday NDVI, SIF, and relative SIF versus Φ_{PSII} on four dates (2022-05-03 to 2022-05-24, corresponding to high-quality midday acquisitions) with linear regression (lines) and error (shading), with respective equations, R^2, and p-values.

geometry of viewing angles and instrument considerations (including spatial stray light, nonuniformity, and radiance calibration stability) are the subject of ongoing SIF imaging research (Albert et al., 2023; van der Tol et al., 2023) and are outside the scope of the current study. However, we emphasize the importance of such corrections in properly interpreting the SIF signal (Aasen et al., 2019; Frankenberg et al., 2018; Sun, Gu, et al., 2023).

2.3. SIF Retrieval

Very few of the photons absorbed by chlorophyll pigments in a leaf are re-emitted as fluorescence, and even fewer of these photons reach a detector after being reabsorbed by the canopy or scattered in the atmosphere. Indeed, the fraction (f_{esc}) of the total SIF emission that reaches the detector is typically only 0%–2% of irradiance (Magney et al., 2020). A variety of methodologies have been developed to retrieve this small signal, many of which use atmospheric absorption features (relatively dark windows of the atmosphere) to better capture emitted photons. The O_2-A Fraunhofer line at approximately 760 nm is deeper than other absorption features and therefore is regularly used for ground-based retrievals (Mohammed et al., 2019). Detailed equations for this methodology, along with a discussion of other Fraunhofer line depth (FLD) methodologies, are presented elsewhere (Damm et al., 2011). Given the imager's spectral range and resolution (Figure S2 in Supporting Information S1), it could be used to retrieve SIF in both the O_2-A and O_2-B absorption features via 3FLD, improved-FLD (Alonso et al., 2008), singular value decomposition (Guanter et al., 2012), spectral fitting (Miao et al., 2018) and band shape fitting (van der Tol et al., 2023) techniques. In this study, we use the 3-FLD method in the O_2-A band at 760 nm to retrieve the fraction of leaf-level SIF at 760 nm that escapes the canopy and reaches the detector (SIF_{760}), which we will refer to as 'SIF' in this paper for simplicity:

$$SIF = SIF_{760} = \frac{L_{O_2} - \frac{E_1}{w_{21}E_{21}+w_{22}E_{22}} \times (w_{21}L_L + w_{22}L_R)}{1 - \frac{E_1}{w_{21}E_{21}+w_{22}E_{22}}} \quad (3)$$

where $w_{21} = \frac{\lambda_R - \lambda_{O_2}}{\lambda_R - \lambda_L}$ and $w_{22} = \frac{\lambda_{O_2} - \lambda_L}{\lambda_R - \lambda_L}$.

In Equation 3, L_L and L_R represent radiance to the left and right of the O_2-A Fraunhofer line over vegetation, respectively, and L_{O_2} represents radiance within the O_2-A absorption feature over vegetation. E_{22} and E_{21} represent radiance to the left and right of the O_2-A absorption feature over the reference white panel, respectively, and E_1 represents radiance within the O_2-A band over the white panel. λ_L, λ_R, and λ_{O_2} are wavelength positions in nanometers (nm) of the bands on the left and right shoulders and within the Fraunhofer line at 760 nm, respectively (Figure S2 in Supporting Information S1).

Due to the high spectral resolution of the imager, several spectral bands fall within the O_2-A absorption feature. Consequently, we performed a sensitivity analysis to quantify the effect of averaging over multiple bands as inputs to the 3-FLD method. The details and outcomes of this analysis are discussed in the Supporting Information S1.

Variations in SIF are closely linked to irradiance and f_{esc}. To account for irradiance and canopy structure effects, we also calculate relative SIF (unitless) using total reflected radiance surrounding the absorption feature ($RAD_{757-762}$) (Butterfield et al., 2023; Pierrat et al., 2021, 2022):

$$relative\ SIF = \frac{SIF_{760}}{RAD_{757\text{-}762}} \quad (4)$$

Midday retrievals of $RAD_{757-762}$ and SIF_{760} are shown in Figure S4 in Supporting Information S1. Over its 670–780 nm range, imager data can also be used to calculate NDVI. Red and near-infrared radiances were calculated by averaging bands across 670–680 and 770–780 nm, respectively. As NDVI distinguishes vegetated from non-vegetated surfaces, low NDVI pixels (<0.5) were masked out. In addition, pixels with low NIR (<8 mW cm^{-2} μm^{-1} sr^{-1}, representing the bottom 33% NIR quantile averaged over the season) were masked out to exclude non-vegetated scaffolding at the testbed site. Acquisitions were taken only when the solar azimuth angle was >80° to avoid uncertainty arising from low-light conditions (Pierrat et al., 2021). Images were bilinearly

resampled to lower resolution (aggregating over 4 neighboring pixels) to reduce the effects of wind, which in some instances created blurring between neighboring pixels. Aggregated pixel size was about 0.5 cm.

3. Results and Discussion

3.1. Seasonal and Diurnal Cycles

At the testbed, both NDVI and relative SIF steadily decline over the course of the dry season as vegetation experiences senescence (Figures 2 and 3), reaching their lowest mean values on 2022-05-24. Midday depressions in relative SIF are visible on the first two dates (2022-04-18 and 2022-05-03), reaching local minima around 13:00 (Figure 3). In previous studies, SIF was also found to diminish at peak irradiance and VPD, likely due to an increase in non-photochemical quenching under stressful conditions (e.g., water stress), photosynthetic electron transport saturation, and stomatal closure (Wu et al., 2022; Loayza et al., 2023; Y. Zhang et al., 2023; Siegmann et al., 2021). Midday minima may also be attributed to the influence of sun-sensor geometry (Nichol et al., 2019), although small phase angles have been shown to have minimal effects (Wong et al., 2023).

Throughout the time series, NDVI is fairly constant over the course of the day, with little diurnal variation, while relative SIF exhibits significant diurnal variability. The relationship between NDVI and SIF is nonlinear, with NDVI saturating while SIF continues to increase, especially on 2022-04-18 and 2022-05-03 (Figure 3). This pattern may be due to SIF's strong correlation with irradiance. It also may demonstrate that SIF is linked to diurnal changes in plant function and contains additional and complementary information to NDVI, which primarily captures vegetation structure and does not significantly vary throughout the day. However, this relationship becomes increasingly linear, with a diminishing slope, as the dry-down progresses and both NDVI and SIF values decrease. The relationship between relative SIF and NDVI is more pronounced on 2022-04-18 and 2022-05-03, with some NDVI saturation at high values. Relative SIF displays more linear relationships with NDVI throughout the time series.

3.2. Correlation Analysis

Midday relative SIF exhibits a significant correlation with leaf-level physiology on 2022-05-09 ($p = 0.013$, $R^2 = 0.74$). The correlation is less strong on 2022-04-03 ($p = 0.07$, $R^2 = 0.51$) and diminishes further on the final two days of acquisitions (Figure 4). These results demonstrate the instrument's ability to delineate differences in relative SIF over space and its technological advantage over point estimates of SIF from other instruments. On 2022-04-18, midday SIF retrievals did not align temporally with LiCOR measurements, resulting in a weak correlation.

Over the course of the dry down, the magnitude of SIF, relative SIF and Φ_{PSII} among all measured plants decreased, as expected given the progression of senescence. The lack of significant relationships may be due to differences in senescence status and species. For example, mean daily values of relative SIF and Φ_{PSII} from *Rumex crispus* track each other well on an individual plant basis, while *Melica Californica* shows less agreement (Figure S5 in Supporting Information S1). Although only one midday acquisition (2022-05-09) is significant ($p < 0.05$), these data suggest SIF retrievals from the imager can differentiate leaf-level physiology between individual plants across space. More frequent LiCOR sampling would improve prediction power in future work. Across the entire season, midday relative SIF outperforms both NDVI and SIF in predicting Φ_{PSII} ($p < 0.01$ and $R^2 = 0.33$, Figure 4e).

Together, these results demonstrate that SIF retrieved from the imager is capable of not only detecting leaf-level physiology but also distinguishing changes in physiological function across space and time. The decrease in R^2 values throughout the dry down also suggests vegetation health and stress levels affect the relationship between relative SIF and leaf-level physiology, which is stronger in verdant, well-watered plants and diminish as vegetation senesces and vapor pressure deficit increases. These results are expected given the decoupling between SIF and ecosystem function observed under increasing stress conditions (Magney et al., 2020).

Diurnal relative SIF measurements scale well with GPP estimates derived from the eddy covariance tower at Tonzi Ranch (Figure S6 in Supporting Information S1). Relative SIF closely tracks changes in GPP throughout the course of the day, while PAR, TA, and VPD exhibit smooth diurnal curves. For example, both GPP and relative SIF undergo a midday depression at 13:00. A linear regression between GPP and relative SIF confirms this relationship is significant ($p = 0.04$) and correlated ($R^2 = 0.48$). A hysteresis effect, with higher relative SIF values earlier in the

day, agrees with previous work (Pinto et al., 2016; Siegmann et al., 2021). Discrepancies between GPP and relative SIF may be due to variations in the footprint of the eddy covariance tower, which deviates from its average footprint under varying wind conditions (Kljun et al., 2015). Divergences between GPP and relative SIF may also be a result of tower data aggregation to half-hourly increments. Additional data collection at this or other eddy covariance flux tower sites is needed to confirm the conclusions of this study.

4. Conclusions

The Headwall ultra-hyperspectral imager, among the first commercially available SIF imaging instruments, provides a novel approach to quantifying plant physiology across leaf, plant, and landscape scales. Unlike vegetation indices that primarily detect changes in vegetation structure (e.g., NDVI), SIF varies on a minute-by-minute basis, capturing changes in ecosystem function in real-time, while variations in NDVI emerge only at the seasonal scale. Leaf-level measurements show significant ($p < 0.01$) relationships between imager-derived SIF and Φ_{PSII} on one day, suggesting the instrument can successfully differentiate leaf-level physiology over space and time. However, these relationships become decoupled with increasing environmental stress and plant senescence, as expected given the current understanding of energy partitioning within chloroplasts (Magney et al., 2020; Porcar-Castell et al., 2014), and vary between species. SIF also significantly correlates with GPP estimates at a grassland site ($p = 0.042$).

There is much more work to be done with this and similar instruments. Future studies should consider additional approaches to account for canopy structure, sun-sensor geometries, viewing angle and lens effects, and hotspots (Z. Zhang et al., 2020). More frequent leaf-level LiCOR measurements, a larger imaging data set, and additional work on the SIF-GPP relationship are needed to confirm the initial results presented here. Additional SIF retrieval algorithms, such as the improved FLD, singular value decomposition, and spectral fitting, should be pursued. A methodology to retrieve fluorescence yield with the imager would enable better characterization of leaf-level processes. In addition, joint campaigns using multiple SIF instruments would improve retrieval algorithms by creating a universal standard. Imaging technology in particular has potential synergy with radiative transfer modeling (and especially 3D models (Malenovský et al., 2021)), which would provide an increased understanding of the fate of photons absorbed by vegetation across space and time (van der Tol et al., 2016; Yang et al., 2017). Finally, concurrent measurement of non-photochemical quenching may explain increased decoupling between SIF and leaf-level physiology with increasing stress (Maguire et al., 2020; Xu et al., 2021).

Overall, these findings support the use of SIF imaging to better capture leaf-level physiology, improve understanding of ecosystem function, and expand the community's understanding of nonlinearities between SIF and photosynthesis in water-limited ecosystems across time and space. The instrument's high spatial resolution avoids mixed pixels, enabling the imaging of individual plants and their leaves within one scene. Our results demonstrate an advancement in remote sensing of plant physiology from the leaf to the ecosystem.

Data Availability Statement

One day of radiance data from the hyperspectral imager, along with Python software and documentation for initial processing of these data into NDVI, NIRvR, and SIF, is currently available online (Ruehr, 2023).

Acknowledgments
SR acknowledges support from a NASA FINESST fellowship 80NSSC22K1448 and the UC Berkeley Carol Baird Fieldwork Grant. NF and CC were supported by a Laboratory Directed Research and Development (LDRD) funding from Lawrence Berkeley National Laboratory, provided by the Director, Office of Science, of the U.S. Department of Energy under Contract No. DE-AC02-05CH11231. TFK was supported by a DOE ECRP Award DE-SC0021023 and a NASA Carbon Cycle Science Award 80NSSC21K1705. LPA was supported in part by NASA Carbon Cycle Science Award 80NSSC21K1707. The funding for the SMARTSoils testbed is supported by the U.S. Department of Energy, Office of Science, Office of Biological and Environmental Research, Watershed Function Scientific Focus Area (SFA) and Belowground Biogeochemistry SFA to Lawrence Berkeley National Laboratory. Thank you to Joseph Verfaillie, Ann Scheliga, Kyle Delwiche, Tyler Goldstein, Megan Hur, and Gabriel Wheaton for field assistance.

References

Aasen, H., Van Wittenberghe, S., Sabater Medina, N., Damm, A., Goulas, Y., Wieneke, S., et al. (2019). Sun-induced chlorophyll fluorescence II: Review of passive measurement setups, protocols, and their application at the leaf to canopy level. *Remote Sensing*, *11*(8), 927. https://doi.org/10.3390/rs11080927

Albert, L. P., Cushman, K. C., Zong, Y., Allen, D. W., Alonso, L., & Kellner, J. R. (2023). Sensitivity of solar-induced fluorescence to spectral stray light in high resolution imaging spectroscopy. *Remote Sensing of Environment*, *285*, 113313. https://doi.org/10.1016/j.rse.2022.113313

Alonso, L., Gomez-Chova, L., Vila-Frances, J., Amoros-Lopez, J., Guanter, L., Calpe, J., & Moreno, J. (2008). Improved fraunhofer line discrimination method for vegetation fluorescence quantification. *IEEE Geoscience and Remote Sensing Letters*, *5*(4), 620–624. https://doi.org/10.1109/LGRS.2008.2001180

Belwalkar, A., Poblete, T., Longmire, A., Hornero, A., & Zarco-Tejada, P. (2021). Comparing the retrieval of chlorophyll fluorescence from two airborne hyperspectral imagers with different spectral resolutions for plant phenotyping studies. In *2021 IEEE international geoscience and remote sensing symposium IGARSS* (pp. 5845–5848). https://doi.org/10.1109/IGARSS47720.2021.9553265

Butterfield, Z., Magney, T., Grossmann, K., Bohrer, G., Vogel, C., Barr, S., & Keppel-Aleks, G. (2023). Accounting for changes in radiation improves the ability of SIF to track water stress-induced losses in summer GPP in a temperate deciduous forest. *Journal of Geophysical Research: Biogeosciences*, *128*(7), e2022JG007352. https://doi.org/10.1029/2022JG007352

Damm, A., Erler, A., Hillen, W., Meroni, M., Schaepman, M. E., Verhoef, W., & Rascher, U. (2011). Modeling the impact of spectral sensor configurations on the FLD retrieval accuracy of sun-induced chlorophyll fluorescence. *Remote Sensing of Environment*, *115*(8), 1882–1892. https://doi.org/10.1016/j.rse.2011.03.011

Frankenberg, C., Köhler, P., Magney, T. S., Geier, S., Lawson, P., Schwochert, M., et al. (2018). The chlorophyll fluorescence imaging spectrometer (CFIS), mapping far red fluorescence from aircraft. *Remote Sensing of Environment*, *217*, 523–536. https://doi.org/10.1016/j.rse.2018.08.032

Fu, P., Meacham-Hensold, K., Siebers, M. H., & Bernacchi, C. J. (2021). The inverse relationship between solar-induced fluorescence yield and photosynthetic capacity: Benefits for field phenotyping. *Journal of Experimental Botany*, *72*(4), 1295–1306. https://doi.org/10.1093/jxb/eraa537

Guanter, L., Frankenberg, C., Dudhia, A., Lewis, P. E., Gómez-Dans, J., Kuze, A., et al. (2012). Retrieval and global assessment of terrestrial chlorophyll fluorescence from GOSAT space measurements. *Remote Sensing of Environment*, *121*, 236–251. https://doi.org/10.1016/j.rse.2012.02.006

He, L., Magney, T., Dutta, D., Yin, Y., Köhler, P., Grossmann, K., et al. (2020). From the ground to space: Using solar-induced chlorophyll fluorescence to estimate crop productivity. *Geophysical Research Letters*, *47*(7), e2020GL087474. https://doi.org/10.1029/2020GL087474

Kljun, N., Calanca, P., Rotach, M. W., & Schmid, H. P. (2015). A simple two-dimensional parameterisation for flux footprint prediction (FFP). *Geoscientific Model Development*, *8*(11), 3695–3713. https://doi.org/10.5194/gmd-8-3695-2015

Li, X., Xiao, J., He, B., Arain, M. A., Beringer, J., Desai, A. R., et al. (2018). Solar-induced chlorophyll fluorescence is strongly correlated with terrestrial photosynthesis for a wide variety of biomes: First global analysis based on OCO-2 and flux tower observations. *Global Change Biology*, *24*(9), 3990–4008. https://doi.org/10.1111/gcb.14297

Liu, L., Yang, X., Zhou, H., Liu, S., Zhou, L., Li, X., et al. (2018). Evaluating the utility of solar-induced chlorophyll fluorescence for drought monitoring by comparison with NDVI derived from wheat canopy. *The Science of the Total Environment*, *625*, 1208–1217. https://doi.org/10.1016/j.scitotenv.2017.12.268

Loayza, H., Moya, I., Quiroz, R., Ounis, A., & Goulas, Y. (2023). Active and passive chlorophyll fluorescence measurements at canopy level on potato crops. evidence of similitude of diurnal cycles of apparent fluorescence yields. *Photosynthesis Research*, *155*(3), 271–288. https://doi.org/10.1007/s11120-022-00995-8

Ma, S., Xu, L., Verfaillie, J., & Baldocchi, D. (2016). *Tonzi Ranch (US-Ton) dataset (Tech. Rep.)*. Lawrence Berkeley National Lab. (LBNL). AmeriFlux; Univ. of California, Berkeley, CA (United States). https://doi.org/10.17190/AMF/1245971

Magney, T. S., Barnes, M. L., & Yang, X. (2020). On the covariation of chlorophyll fluorescence and photosynthesis across scales. *Geophysical Research Letters*, *47*(23). https://doi.org/10.1029/2020GL091098

Maguire, A. J., Eitel, J. U. H., Griffin, K. L., Magney, T. S., Long, R. A., Vierling, L. A., et al. (2020). On the functional relationship between fluorescence and photochemical yields in complex evergreen needleleaf canopies. *Geophysical Research Letters*, *47*(9), e2020GL087858. https://doi.org/10.1029/2020GL087858

Maguire, A. J., Eitel, J. U. H., Magney, T. S., Frankenberg, C., Köhler, P., Orcutt, E. L., et al. (2021). Spatial covariation between solar-induced fluorescence and vegetation indices from arctic-boreal landscapes. *Environmental Research Letters*, *16*(9), 095002. https://doi.org/10.1088/1748-9326/ac188a

Malenovský, Z., Regaieg, O., Yin, T., Lauret, N., Guilleux, J., Chavanon, E., et al. (2021). Discrete anisotropic radiative transfer modelling of solar-induced chlorophyll fluorescence: Structural impacts in geometrically explicit vegetation canopies. *Remote Sensing of Environment*, *263*, 112564. https://doi.org/10.1016/j.rse.2021.112564

Marrs, J. K., Reblin, J. S., Logan, B. A., Allen, D. W., Reinmann, A. B., Bombard, D. M., et al. (2020). Solar-induced fluorescence does not track photosynthetic carbon assimilation following induced stomatal closure. *Geophysical Research Letters*, *47*(15). https://doi.org/10.1029/2020GL087956

Martini, D., Sakowska, K., Wohlfahrt, G., Pacheco-Labrador, J., van der Tol, C., Porcar-Castell, A., et al. (2022). Heatwave breaks down the linearity between sun-induced fluorescence and gross primary production. *New Phytologist*, *233*(6), 2415–2428. https://doi.org/10.1111/nph.17920

Miao, G., Guan, K., Yang, X., Bernacchi, C. J., Berry, J. A., DeLucia, E. H., et al. (2018). Sun-induced chlorophyll fluorescence, photosynthesis, and light use efficiency of a soybean field from seasonally continuous measurements. *Journal of Geophysical Research: Biogeosciences*, *123*(2), 610–623. https://doi.org/10.1002/2017JG004180

Mohammed, G. H., Colombo, R., Middleton, E. M., Rascher, U., van der Tol, C., Nedbal, L., et al. (2019). Remote sensing of solar-induced chlorophyll fluorescence (SIF) in vegetation: 50 years of progress. *Remote Sensing of Environment*, *231*, 111177. https://doi.org/10.1016/j.rse.2019.04.030

Nichol, C. J., Drolet, G., Porcar-Castell, A., Wade, T., Sabater, N., Middleton, E. M., et al. (2019). Diurnal and seasonal solar induced chlorophyll fluorescence and photosynthesis in a boreal Scots pine canopy. *Remote Sensing*, *11*(3), 273. https://doi.org/10.3390/rs11030273

Paynter, I., Cook, B., Corp, L., Nagol, J., & McCorkel, J. (2020). Characterization of FIREFLY, an imaging spectrometer designed for remote sensing of solar induced fluorescence. *Sensors*, *20*(17), 4682. https://doi.org/10.3390/s20174682

Pierrat, Z., Magney, T., Parazoo, N. C., Grossmann, K., Bowling, D. R., Seibt, U., et al. (2022). Diurnal and seasonal dynamics of solar-induced chlorophyll fluorescence, vegetation indices, and gross primary productivity in the boreal forest. *Journal of Geophysical Research: Biogeosciences*, *127*(2), e2021JG006588. https://doi.org/10.1029/2021JG006588

Pierrat, Z., Magney, T. S., Cheng, R., Maguire, A., Wong, C. Y. S., Nehemy, M., et al. (2024). The biological basis for using optical signals to track evergreen needleleaf photosynthesis. *BioScience*, *74*(3), 130–145. https://doi.org/10.7916/hqzs-hv62

Pierrat, Z., Nehemy, M. F., Roy, A., Magney, T., Parazoo, N. C., Laroque, C., et al. (2021). Tower-based remote sensing reveals mechanisms behind a two-phased spring transition in a mixed-species boreal forest. *Journal of Geophysical Research: Biogeosciences*, *126*(5), e2020JG006191. https://doi.org/10.1029/2020JG006191

Pinto, F., Damm, A., Schickling, A., Panigada, C., Cogliati, S., Müller-Linow, M., et al. (2016). Sun-induced chlorophyll fluorescence from high-resolution imaging spectroscopy data to quantify spatio-temporal patterns of photosynthetic function in crop canopies. *Plant, Cell and Environment*, *39*(7), 1500–1512. https://doi.org/10.1111/pce.12710

Porcar-Castell, A., Malenovský, Z., Magney, T., Van Wittenberghe, S., Fernández-Marín, B., Maignan, F., et al. (2021). Chlorophyll a fluorescence illuminates a path connecting plant molecular biology to Earth-system science. *Nature Plants*, *7*(8), 998–1009. https://doi.org/10.1038/s41477-021-00980-4

Porcar-Castell, A., Tyystjärvi, E., Atherton, J., van der Tol, C., Flexas, J., Pfündel, E. E., et al. (2014). Linking chlorophyll a fluorescence to photosynthesis for remote sensing applications: Mechanisms and challenges. *Journal of Experimental Botany*, *65*(15), 4065–4095. https://doi.org/10.1093/jxb/eru191

Rascher, U., Alonso, L., Burkart, A., Cilia, C., Cogliati, S., Colombo, R., et al. (2015). Sun-induced fluorescence – A new probe of photosynthesis: First maps from the imaging spectrometer HyPlant. *Global Change Biology*, *21*(12), 4673–4684. https://doi.org/10.1111/gcb.13017

Rossini, M., Nedbal, L., Guanter, L., Ač, A., Alonso, L., Burkart, A., et al. (2015). Red and far red sun-induced chlorophyll fluorescence as a measure of plant photosynthesis. *Geophysical Research Letters*, *42*(6), 1632–1639. https://doi.org/10.1002/2014GL062943

Ruehr, S. (2023). Hyperspectral imager acquisitions from SMART soils test bed, 2022-04-18 (1.0). [Dataset]. *Zenodo*. https://doi.org/10.5281/zenodo.10246787

Siegmann, B., Cendrero-Mateo, M. P., Cogliati, S., Damm, A., Gamon, J., Herrera, D., et al. (2021). Downscaling of far-red solar-induced chlorophyll fluorescence of different crops from canopy to leaf level using a diurnal data set acquired by the airborne imaging spectrometer HyPlant. *Remote Sensing of Environment*, *264*, 112609. https://doi.org/10.1016/j.rse.2021.112609

Simmer, C., Thiele-Eich, I., Masbou, M., Amelung, W., Bogena, H., Crewell, S., et al. (2015). Monitoring and modeling the terrestrial system from pores to catchments: The transregional collaborative research center on patterns in the soil–vegetation–atmosphere system. *Bulletin of the American Meteorological Society*, *96*(10), 1765–1787. https://doi.org/10.1175/BAMS-D-13-00134.1

Sun, Y., Frankenberg, C., Wood, J. D., Schimel, D. S., Jung, M., Guanter, L., et al. (2017). OCO-2 advances photosynthesis observation from space via solar-induced chlorophyll fluorescence. *Science*, *358*(6360), eaam5747. https://doi.org/10.1126/science.aam5747

Sun, Y., Gu, L., Wen, J., van der Tol, C., Porcar-Castell, A., Joiner, J., et al. (2023a). From remotely sensed solar-induced chlorophyll fluorescence to ecosystem structure, function, and service: Part I—Harnessing theory. *Global Change Biology*, *29*(11), 2926–2952. https://doi.org/10.1111/gcb.16634

Sun, Y., Wen, J., Gu, L., Joiner, J., Chang, C. Y., van der Tol, C., et al. (2023b). From remotely-sensed solar-induced chlorophyll fluorescence to ecosystem structure, function, and service: Part II—Harnessing data. *Global Change Biology*, *29*(11), 2893–2925. https://doi.org/10.1111/gcb.16646

van der Tol, C., Julitta, T., Yang, P., Sabater, N., Reiter, I., Tudoroiu, M., et al. (2023). Retrieval of chlorophyll fluorescence from a large distance using oxygen absorption bands. *Remote Sensing of Environment*, *284*, 113304. https://doi.org/10.1016/j.rse.2022.113304

van der Tol, C., Rossini, M., Cogliati, S., Verhoef, W., Colombo, R., Rascher, U., & Mohammed, G. (2016). A model and measurement comparison of diurnal cycles of sun-induced chlorophyll fluorescence of crops. *Remote Sensing of Environment*, *186*, 663–677. https://doi.org/10.1016/j.rse.2016.09.021

Verma, M., Schimel, D., Evans, B., Frankenberg, C., Beringer, J., Drewry, D. T., et al. (2017). Effect of environmental conditions on the relationship between solar-induced fluorescence and gross primary productivity at an OzFlux grassland site. *Journal of Geophysical Research: Biogeosciences*, *122*(3), 716–733. https://doi.org/10.1002/2016JG003580

Wang, S., Huang, C., Zhang, L., Lin, Y., Cen, Y., & Wu, T. (2016). Monitoring and assessing the 2012 drought in the great plains: Analyzing satellite-retrieved solar-induced chlorophyll fluorescence, drought indices, and gross primary production. *Remote Sensing*, *8*(2), 61. https://doi.org/10.3390/rs8020061

Wong, C. Y. S., Jones, T., McHugh, D. P., Gilbert, M. E., Gepts, P., Palkovic, A., et al. (2023). Tswift: Tower spectrometer on wheels for investigating frequent timeseries for high-throughput phenotyping of vegetation physiology. *Plant Methods*, *19*(1), 29. https://doi.org/10.1186/s13007-023-01001-5

Wu, G., Guan, K., Jiang, C., Kimm, H., Miao, G., Bernacchi, C. J., et al. (2022). Attributing differences of solar-induced chlorophyll fluorescence (SIF)-gross primary production (GPP) relationships between two c4 crops: Corn and miscanthus. *Agricultural and Forest Meteorology*, *323*, 109046. https://doi.org/10.1016/j.agrformet.2022.109046

Xu, S., Atherton, J., Riikonen, A., Zhang, C., Oivukkamäki, J., MacArthur, A., et al. (2021). Structural and photosynthetic dynamics mediate the response of SIF to water stress in a potato crop. *Remote Sensing of Environment*, *263*, 112555. https://doi.org/10.1016/j.rse.2021.112555

Yang, P., Verhoef, W., & van der Tol, C. (2017). The mSCOPE model: A simple adaptation to the SCOPE model to describe reflectance, fluorescence and photosynthesis of vertically heterogeneous canopies. *Remote Sensing of Environment*, *201*, 1–11. https://doi.org/10.1016/j.rse.2017.08.029

Zhang, J., Xiao, J., Tong, X., Zhang, J., Meng, P., Li, J., et al. (2022). NIRv and SIF better estimate phenology than NDVI and EVI: Effects of spring and autumn phenology on ecosystem production of planted forests. *Agricultural and Forest Meteorology*, *315*, 108819. https://doi.org/10.1016/j.agrformet.2022.108819

Zhang, Y., Fang, J., Smith, W. K., Wang, X., Gentine, P., Scott, R. L., et al. (2023). Satellite solar-induced chlorophyll fluorescence tracks physiological drought stress development during 2020 southwest US drought. *Global Change Biology*, *29*(12), 3395–3408. https://doi.org/10.1111/gcb.16683

Zhang, Z., Zhang, Y., Zhang, Q., Chen, J. M., Porcar-Castell, A., Guanter, L., et al. (2020). Assessing bi-directional effects on the diurnal cycle of measured solar-induced chlorophyll fluorescence in crop canopies. *Agricultural and Forest Meteorology*, *295*, 108147. https://doi.org/10.1016/j.agrformet.2020.108147